Agricultural and Forest Meteorology 244–245 (2017) 57–71

Contents lists available at ScienceDirect

Agricultural and Forest Meteorology

journal homepage: www.elsevier.com/locate/agrformet

Comparison of different satellite bands and vegetation indices for estimation of soil organic matter based on simulated spectral configuration

Xiuliang Jin, Kaishan Song*, Jia Du, Huanjun Liu, Zhidan Wen

Key Laboratory of Wetland Ecology and Environment, Northeast Institute of Geography and Agroecology, Chinese Academy of Sciences, Changchun 130102, Jilin, China

ARTICLE INFO

Keywords:
Soil organic matter content
Spectral response function
Optimal band algorithm
Particle swarm optimization
Support vector machine

ABSTRACT

Soil organic matter content (SOM) is an important indicator of soil productivity that governs biological, chemical, and physical processes in the soil environment. Previous studies have shown that remote sensing data provide useful information for SOM estimation in different soil types. However, no studies have estimated SOM based on simulated spectral configurations of different satellite sensors. Further study is required to investigate whether SOM estimation accuracy can be improved by combining data from different satellite sensors and developing appropriate algorithms. Therefore, this study investigated new methods for SOM estimation with the following three objectives: (1) analyze the reflectance changes of simulated bands for different SOMs using the spectral response function of various satellite sensors; (2) develop optimal difference index (ODI), optimal ratio index (ORI), optimal normalized vegetation difference index (ONDVI), and optimal enhanced vegetation index (OEVI) algorithms for estimating SOM based on simulated band reflectance; (3) evaluate all bands, ODI, ORI, ONDVI, and OEVI for all simulated bands derived from the data of each satellite, and then combine the simulated data to estimate SOM using the particle swarm optimization (PSO)-support vector machine (SVM) algorithm. The OEVI analysis of simulated WorldView-2 data provided the best SOM estimation accuracy (R^2 = 0.43 and RMSE = 2.62%). The OEVI and ODI algorithms provided better estimation accuracy of SOM from the different simulated satellite data than the ORI and ONDVI algorithms. The best estimation accuracy of SOM was achieved using the PSO-SVM algorithm and simulated WorldView-2 data (R^2 = 0.77, RMSE = 1.66%, and AIC = 99.62). Combination of simulated bands 4–9 of ASTER data and all bands, ODI, ORI, ONDVI, and OEVI of WorldView-2 data provided optimum SOM estimation results (R^2 = 0.82, RMSE = 1.41%, AIC = 82.86). The results indicate that a combination of different satellite data and the PSO-SVM algorithm significantly improves the estimation accuracy of SOM.

1. Introduction

Soil organic matter content (SOM) affects soil quality and crop growth, and controls biological, chemical, and physical processes in the soil environment (Fleming et al., 2004; Seely et al., 2010; Six and Paustian, 2014). Soil productivity and the carbon cycle can be improved by SOM (Prescott et al., 2000). SOM modeling provides useful information for crop growers because it generates detailed estimations of spatial distributions and variations in SOM, which can be used to improve field management in precision agriculture.

Traditional soil sampling and analysis methods are used to measure SOM. Although these methods confer high accuracy spot measurements, it cannot be used to rapidly estimate SOM over wider areas because it requires relatively longer time and substantial cost. Therefore, there is a pressing need to develop a rapid and accurate method for SOM estimation on a regional scale with low cost. Remote sensing technology provides an effective method for estimating spatial changes in SOM on a regional scale.

Bowers and Hanks (1965) first studied the relationship between soil spectral reflectance and soil properties, and acquired spectral data for different soil types. Many studies have investigated the relationship between SOM and soil spectral data for different soil types (Krishnan et al., 1980; Xu and Dai, 1980; Baumgardner et al., 1985; Palacio-Oruetaand Ustin, 1998; Shepherd and Walsh, 2002; Rosselet al., 2006; Zhou et al., 2008; Guoet al., 2013; Kweon and Maxton, 2013; Qi et al., 2014; Liu et al., 2015; Jin et al., 2016). The results suggested that the overall spectral reflectance decreased gradually with increasing SOM within the 350–2500 nm spectral regions (Dalal and Henry, 1986; Irons et al., 1989).

The wavelengths around 410, 447, 491, 520, 540, 550, 560, 570, and 660 nm; 960 and 1100 nm; and 1400, 1900, 1720, 2180, 2309, 1744, 1870, and 2052 nm are located in the visible (VIS), near-infrared

* Corresponding author.
E-mail address: songks@iga.ac.cn (K. Song).

http://dx.doi.org/10.1016/j.agrformet.2017.05.018
Received 12 July 2016; Received in revised form 17 May 2017; Accepted 28 May 2017
Available online 03 June 2017

(NIR), and shortwave infrared (SWIR) spectral regions, respectively. The VIS spectral region was used to estimate SOM because the reflectance in this region is reduced by SOM (Daniel et al., 2004; Brown et al., 2006; Xie et al., 2005; Stamatiadis et al., 2005; Rossel et al., 2006). The NIR and SWIR spectral regions are very sensitive to SOM (Dalal and Henry, 1986; Sudduth and Hummel, 1991; Palacio-Orueta and Ustin, 1998; Shepherd and Walsh, 2002; Daniel et al., 2004). Results have indicated sensitive spectral regions of soil spectral data that are worthy of further research, development, and applications related to SOM (Sudduth and Hummel, 1991; Shepherd and Walsh, 2002; Rossel et al., 2006; Kweonand Maxton, 2013; Qi et al., 2014; Jin et al., 2016). Therefore, numerous studies have quantitatively estimated SOM for different soil types using spectral data.

The absorption ratio indices (ARIs) were used to estimate SOM in different soil types; the results indicated that ARIs had good regression relationships with SOM (Krishnan et al., 1980). Previous studies have indicated that the VIS, NIR, and SWIR spectral regions can be used to detect SOM (Brown et al., 2006; Daniel et al., 2004; Palacio-Orueta and Ustin, 1998), and models based on these sensitive spectral regions have been developed to estimate SOM (Rossel et al., 2006; Qi et al., 2014; Jin et al., 2016). A portable spectrophotometer was used to estimate SOM over a wide geographical region, and the results showed that the reflectance of NIR spectral regions had a good relationship with SOM (R^2 = 0.88, standard error of prediction = 5.31%; Hummel et al., 2001). Daniel et al. (2004) developed a polynomial-based method to estimate SOM using the VIS-NIR spectral region; the results suggested that wavelengths at 520, 960, and 1120 nm were very sensitive to changes in SOM (R^2 = 0.59–0.64).

McCarty and Reeves (2006) applied NIR diffuse reflectance spectroscopy to estimate SOM on regional and global scales. Spectral reflectance of the OMIS-1 sensor together with measurements using the ASD Field Spec FR spectrophotometer have been used to evaluate estimations of SOM (Zhou et al., 2008).

Liu et al. (2009) built a model to estimate SOM using spectral data. The sensitivity of spectral reflectance to SOM was analyzed to estimate topsoil SOM in undergoing desertification areas, and the results revealed strong correlation between the first derivative of reciprocal reflectance at 835 nm [$D(1/R_{835})$] and SOM with R^2 = 0.88 and RMSE = 0.48% (Gao et al., 2011). Kweon and Maxton (2013) determined the sensitive wavelengths for SOM, and then estimated SOM using partial least squares regression. Jin et al. (2016) estimated SOM in the Sanjiang Plain using the optimal band algorithm, grey relational analysis (GRA), and artificial neural network (ANN) analysis; the results showed that GRA-ANN analyses improved the estimation accuracy of SOM based on the selected spectral parameters.

These aforementioned studies showed that spectral data provide useful information for SOM estimation in different soil types. However, no studies have estimated SOM based on the simulated spectral configurations of different satellite sensors. Further study is required to evaluate SOM estimations using data from different satellite sensors, and to develop appropriate algorithms for combining these satellite data and optimizing the estimates. The Sanjiang Plain is an important grain production region of China located in the black-soil region of Northeast China. The spatial distribution of SOM is highly heterogeneous in this region, which presents considerable challenges for rapid and accurate estimations of SOM on a regional scale. SOM itself does not enhance grain production directly; increasing SOM improves the soil nutrient and water holding capacity, which may indirectly improve grain yield and more importantly, grain yield stability and quality thus promoting economic and food security (Fleming et al., 2004; Seely et al., 2010).

The objectives of this study were to (1) analyze the reflectance changes of simulated bands for different SOM using the spectral response function of various satellite sensors; (2) develop optimal index algorithms and evaluate single sources (band reflectance), optimal indexes, or combinations of different simulated data estimation using particle swarm optimization (PSO)-support vector machine (SVM) algorithm to estimate SOM. The optimal indexes include the optimal difference index (ODI), optimal ratio index (ORI), optimal normalized vegetation difference index (ONDVI), and optimal enhanced vegetation index (OEVI). The results of this study provide a useful guideline for SOM estimation in the black-soil region of Northeast China using different satellite data.

2. Material and methods

2.1. Study region

The study region is situated in the Sanjiang Plain (45°01′N – 48°27′N, 130°13′E – 135°05′E), Northeast China (Fig. S1). It has a typical semi-humid continental climate. The annual amount of sunshine is 2400–2500 h. The average minimum and maximum temperature is from −21 °C to −18 °C in January and from 21 °C to 23 °C in July. The average annual precipitation is 500–650 mm. The primary crops under cultivation are rice, soybean, corn, and wheat.

2.2. Collection of soil organic matter

A manually operated soil auger was used to obtain soil surface (0–20 cm) samples. The diameter of soil cores was 3.8 cm. Soil samples were taken randomly based on prior knowledge of within-field variability. Five soil samples for each plot were then combined into one homogenized composite sample. The collected soil samples were kept in a sealed package for later spectral measurements and SOM content analyses in the laboratory. A total of 237 surface soil samples were obtained from the study region in April 2006. These samples were dried using the oven-drying method (O'Kelly, 2004), and then passed through a 2 mm sieve. Soil organic carbon content (SOC, %) was measured using an elemental analyzer (Vario ELII, Elementar Americas, Inc.). SOC is commonly determined as an indicator of SOM because SOM is difficult to directly measure in the laboratory. A conversion coefficient of 1.724 is routinely used to convert SOC to SOM. The coordinate information at the sampling points was recorded with a GPS device. The spatial distribution of sampling points is shown in Fig. S1. The SOM dataset was randomly allocated into the calibration dataset (n = 160) and the validation dataset (n = 77) using SPSS software (version 16.0, SPSS, IBM, Chicago, USA). The SOM for the calibration dataset ranged from 0.55% to 21.37%, with an average of 5.17% and a standard deviation of 2.88%. Similarly, the corresponding values for the validation dataset were 1.15%, 16.71%, 5.14%, and 3.15%, respectively. The soil types in the Sanjiang Plain primarily consist of dark-brown soil, phaeozems, ablic bleached soil, chernozem, and meadow soil. More detailed description of the properties and genesis of these soil types is provided by Jin et al. (2016).

2.3. Spectral measurements

All soil samples were measured using spectrophotometry. Samples were placed into glass jars (12 cm diameter) to form a 1.8-cm thick layer on the bottom of the jar (1.5 cm is the infinite optical thickness for soil; Liu et al., 2002). To prevent any external influences on the measured spectral data, all glass jars were coated with black ink. A ruler was used to flatten the soil sample surface before spectral measurement. An ASD FieldSpec®3 Portable Spectrometer (Analytical Spectral Devices, Boulder, CO, USA) was used to measure the spectral reflectance of the soil samples in a dark laboratory. A 1000 W halogen lamp was placed 0.7 m from the soil sample at a 30° zenith angle, and was used as the light source for measuring the spectral reflectance of the soil samples. An optical probe was fixed approximately 0.15 m above the surface of the soil sample. Therefore, the field-of-view was 2.1 cm diameter, which was smaller than the diameter of the sample jars. This configuration was used to reduce the fraction of visible

shadows and thereby avoid any effects of surface roughness. A standardized white panel (100% reflectance) was used to calibrate the spectral reflectance. The spectral reflectance of each soil sample was measured a total of ten times during development of the analytical method, and the mean of spectral reflectance was computed and analyzed as the sample spectral reflectance.

2.4. Spectral data processing and smoothing

Photoelectrical processing, transmission, and conversion of the spectroscopy data produced electrical, detector, and optical noise (Rossel and Webster, 2012). These noise sources affected the soil spectral reflectance measurements. In addition, the three primary water vapor absorption wavelengths (1350 − 1416 nm, 1796 − 1970 nm, and 2470 − 2500 nm) were affected by the atmospheric water vapor (Jin et al., 2016), which resulted in energy response differences for high-frequency noise and different wavelengths in the spectral curve. Therefore, it was essential to minimize these noise effects by smoothing the spectral curves. The Savitzky-Golay (SG) smoothing method was used to smooth the soil spectral curves. Data were processed using MATLAB software (version R2012a, MathWorks, Natick, MA, USA). The specific details of data processing for SG smoothing are provided in a review by Rinnan et al. (2009).

2.5. Spectral convolution

The simulated soil spectral data were obtained by convolving the field ASD spectral reflectance measurements with the spectral resolution data of each satellite sensor by means of their respective spectral response functions using the built-in resampling functions in ENVI 5.0 software (Exelis Visual Information Solutions, Boulder, CO, USA). The specific information for satellite sensors and spectral response functions are presented in Table S1 and Fig. S2, respectively. The visible and near-infrared bands were considered only because some satellite sensors did not include data for a shortwave infrared band.

2.6. Optimal band algorithm

The contour map approach was used to efficiently select the optimal spectral band combination for different satellite sensors, and for developing new sensors in the future. The results can easily be compared with previous results (Jin et al., 2013). The coefficient of determination (R^2) and root mean square error (RMSE) values of regression equations for vegetation indices and SOM provide comprehensive information on the estimated and predicted power of combining two or three separate spectral bands of satellite data. Therefore, this method was used to build new vegetation indices for estimating SOM with formulas that use the normalized difference vegetation index (NDVI), difference index (DI), ratio index (RI), and enhanced vegetation index (EVI) of the spectral bands in satellite sensor data. Because EVI has three bands, the two-dimensional contour map could not be obtained. Therefore, the estimation model of EVI was computed as the regression model. All possible optimal NDVI, DI, RI, and EVI combinations were obtained using a code developed in MATLAB. The regression equations for spectral indices and SOM estimates were determined based on this code.

2.7. Particle swarm optimization (PSO)–support vector machine (SVM)

2.7.1. Particle swarm optimization algorithm

Kennedy and Eberhart (1995) proposed a new random global optimization algorithm called particle swarm optimization (PSO), which is based on the foraging behavior of birds. The basic concept of PSO is that every solution of the optimization problem, called a particle, defines a fitness function that measures the degree of excellence of each particle solution. Each particle utilizes its own experience and the experience of other particles in the group, which enables each particle to achieve an optimal solution from the whole space.

Specific details of PSO processing are as follows. (1) Initialize a population (array) of particles with random position and velocities on *d* dimensions in the problem space. (2) For each particle, evaluate the desired optimization fitness function in *d* variables. (3) Compare particle's fitness evaluation with particle's individual optimal solution (*pbest*). If current value is better than *pbest*, then set *pbest* value equal to the current value, and the *pbest* location equal to the current location in *d*-dimensional space. (4) Compare particle's fitness evaluation with the population's global optimal solution (*gbest*). If current value is better than *gbest*, then reset *gbest* to the current particle's array index and value. (5) Change the velocity and position of the particle according to the key equations of PSO (Eberhart and Shi, 2001). (6) Loop to step 2 until a criterion is met, usually a sufficiently good fitness or a maximum number of iterations (generations).

2.7.2. Support vector machine

The core concepts of support vector machine (SVM) include mapping the input vectors to high-dimensional feature space based on a preselected nonlinear mapping using the principle of structural risk minimization, constructing the optimal decision function in this space, replacing the dot product operation in the high-dimensional feature space through clever use of the original space of the kernel function, and simplifying complex calculations (Vapnik, 2013). We refer the reader to the studies of Vapnik and Vapnik, 1998; Vapnik, 2013 for more details about SVM and for the original derivation of the technique. In this study, we selected the radial basis function (RBF) as the kernel function for the SVM model. The RBF kernel function can be used as a universal kernel function that can be applied to any sample distribution by selecting the parameters. Overall, the current RBF kernel function is the most widely applied kernel function in the SVM model.

2.7.3. Combination of the PSO and SVM algorithms and application of the method

Two parameters (*C*, punishment parameter; γ, kernel function parameter) are important and directly influence the accuracy of the prediction model when the regression equation is used to establish the SVM model (Vapnik and Vapnik, 1998; Vapnik, 2013). Searching for the best *C* and γ is a problem of model selection. Because PSO is a rapid and global optimization solution, it is used to find the optimal *C* and γ for SVM.

The procedural steps for estimating SOM based on PSO-SVM are as follows:

(1) Normalize the dataset. Allocate the dataset into the calibration and validation datasets.
(2) Perform initial configuration, including setting group size (25), number of iterations (300), velocity of the initial particle (c1 = 1.5, c2 = 1.7), minimum and maximum values of parameter *C* in SVM (0.01, 1000), and minimum and maximum values of parameter γ in SVM (0.01, 1000).
(3) Each individual particle corresponding to *C* and γ were selected to establish the learning model for SVM prediction. The fitness value was calculated for each individual particle to determine the prediction power of the corresponding SVM model. The fitness function is given by

$$f(z_i) = \min(\max(\left\{\frac{x_j - x'_j}{x'_j}\right\}), j = 1,2,\ldots, l) \quad (1)$$

where x_j represents the z_i particle corresponding to the displacement predictive value of the *j*-th test sample; $x'_j$is the measured value of the *j*-th test sample; $j = 1, 2,\ldots l$, is the number of test samples.

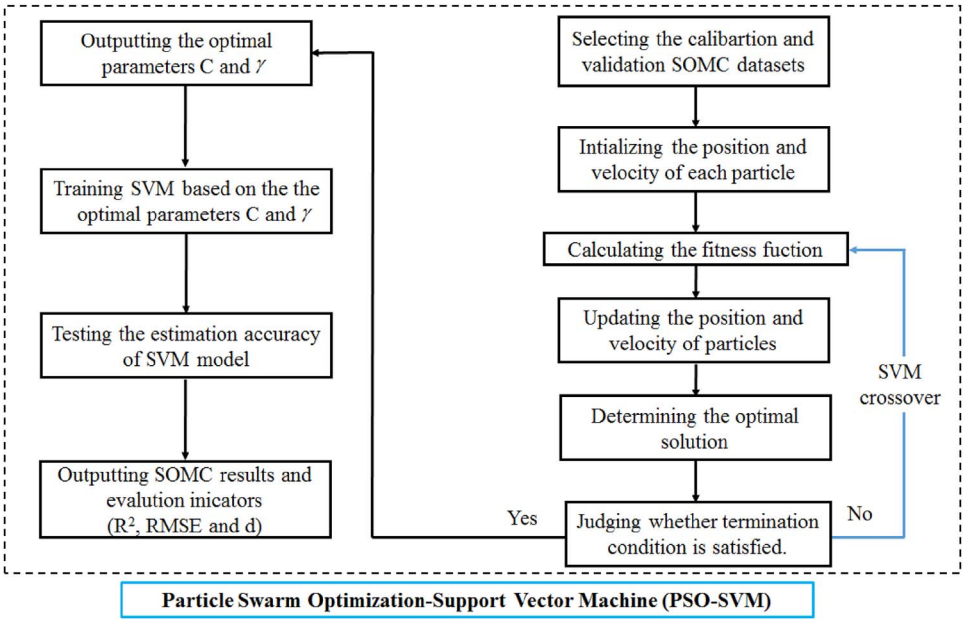

Fig. 1. Flowchart of the particle swarm optimization-support vector machine (PSO-SVM) model for estimating soil organic matter content.

(4) The particle fitness value $f(z_i)$ and the optimal value of this particle $f(pbest_i)$ are compared based on the PSO algorithm. If $f(z_i) < f(pbest_i)$, then the optimal solution of the previous iteration is replaced with the new fitness value, and the particle used in the previous iteration is replaced with a new particle.
(5) The optimal fitness value of each individual particle and the optimal fitness value of all particles are compared. If $f(pbest_i) < f(gbest_i)$, the optimal fitness value of all particles are replaced with the optimal fitness value of each individual particle while preserving the current state of each individual particle.
(6) Determine whether fitness values or iterations meet the selected requirements. If not, conduct a new set of iterations according to Eq. (1). Produce new particles (new solutions), and returning to Step 3. If the new fitness value meets the selected requirements, the calculation is finished, and the optimal parameters C and γ are determined.
(7) The SVM model is established to estimate SOM using the optimal parameters C and γ. The flowchart of the PSO-SVM model is presented in Fig. 1.

2.8. Statistical analysis

The linear and nonlinear regression relationships between SOM and the optimal vegetation indices were analyzed using the calibration dataset (n = 160) and the validation dataset (n = 77). The R^2 and RMSE were used to quantify the estimation accuracy of these optimal vegetation indices. The most accurate regression equations (highest R^2 and lowest RMSE) of the optimal vegetation indices were used to estimate SOM. In addition, the Akaike information criterion (AIC) was calculated to better evaluate the estimation accuracy of the multiple parameter statistical model. The AIC is used to measure the goodness of fit of a statistical model (Arnold, 2010). It describes the trade-off between bias and variance in model construction, or loosely speaking, that of model accuracy and complexity. The equation to calculate AIC was provided by the study of Arnold (2010):

$$AIC = n\log(\frac{RSS}{n}) + 2k \quad (2)$$

Where n is the data sample size, RSS is the residual sum of squares of the fitted model, and k is the number of fitted model parameters.

3. Results

3.1. Simulated band reflectance for different soil organic matter contents

The simulated band reflectance of various satellite sensors had similar spectral shapes under different SOM (Fig. 2). The lowest spectral reflectance was observed in band 1 of the different satellite sensors. The highest spectral reflectance that was observed differed by satellite sensors as follows: band 4 of GeoEye-1 (0.780–0.920 μm) and HJ-1A/B (0.760–0.900 μm); band 5 of RapidEye (0.760–0.850 μm), Landsat TM5 (1.550–1.750 μm), and Landsat TM7 (1.550–1.750 μm); band 7 of ASTER (2.235–2.285 μm) and MODIS (2.105–2.155 μm); and band 8 of WorldView-2 (0.860–1.040 μm). These results indicate that the bands of different satellite sensors had similar spectral shapes, but differed in the spectral reflectance due to the effects of SOM. Because the spectral reflectance was absorbed by SOM (Gaffey et al., 1993; Vasques et al., 2010; Kweon and Maxton, 2013), it decreased gradually with increasing SOM in all bands of the different satellite sensors. The highest and lowest spectral reflectance values were observed at 0.55% and 21.37% SOM, respectively. The results suggested that changes in the spectral reflectance in the visible, near-infrared, and shortwave infrared regions of the satellite sensors primarily determined the simulated band reflectance that was used to estimate SOM.

3.2. Optimal band algorithm for soil organic matter content estimation using different simulated satellite data

The correlations between SOM and the DI, RI, NDVI, and EVI values from different simulated satellite data were analyzed using the optimal band algorithm. The highest correlation between SOM and the optimal difference index (ODI) was observed for bands 1 and 2 (the soil organic matter absorption region, $R^2 > 0.30$) of the different simulated satellite data (Fig. 3). The selected spectral region (bands 1 and 2) of these satellite sensors was essentially the same, except for that of the ASTER, MODIS, and WorldView-2 sensors (Table S1). Bands 1 and 2 were used to estimate SOM using the regression model. The results showed that the ODI derived from WorldView-2 had the highest SOM estimation accuracy (R^2 = 0.43 and RMSE = 2.648%, Fig. 3, Table S2). The ODI derived from ASTER had the lowest SOM estimation accuracy (R^2 = 0.4417 and RMSE = 2.959%). The aggregated RI, NDVI, and EVI datasets were subjected to ODI analysis (Figs. 4 and 5, Table S2).

The bands with highest correlation between the optimal ratio index

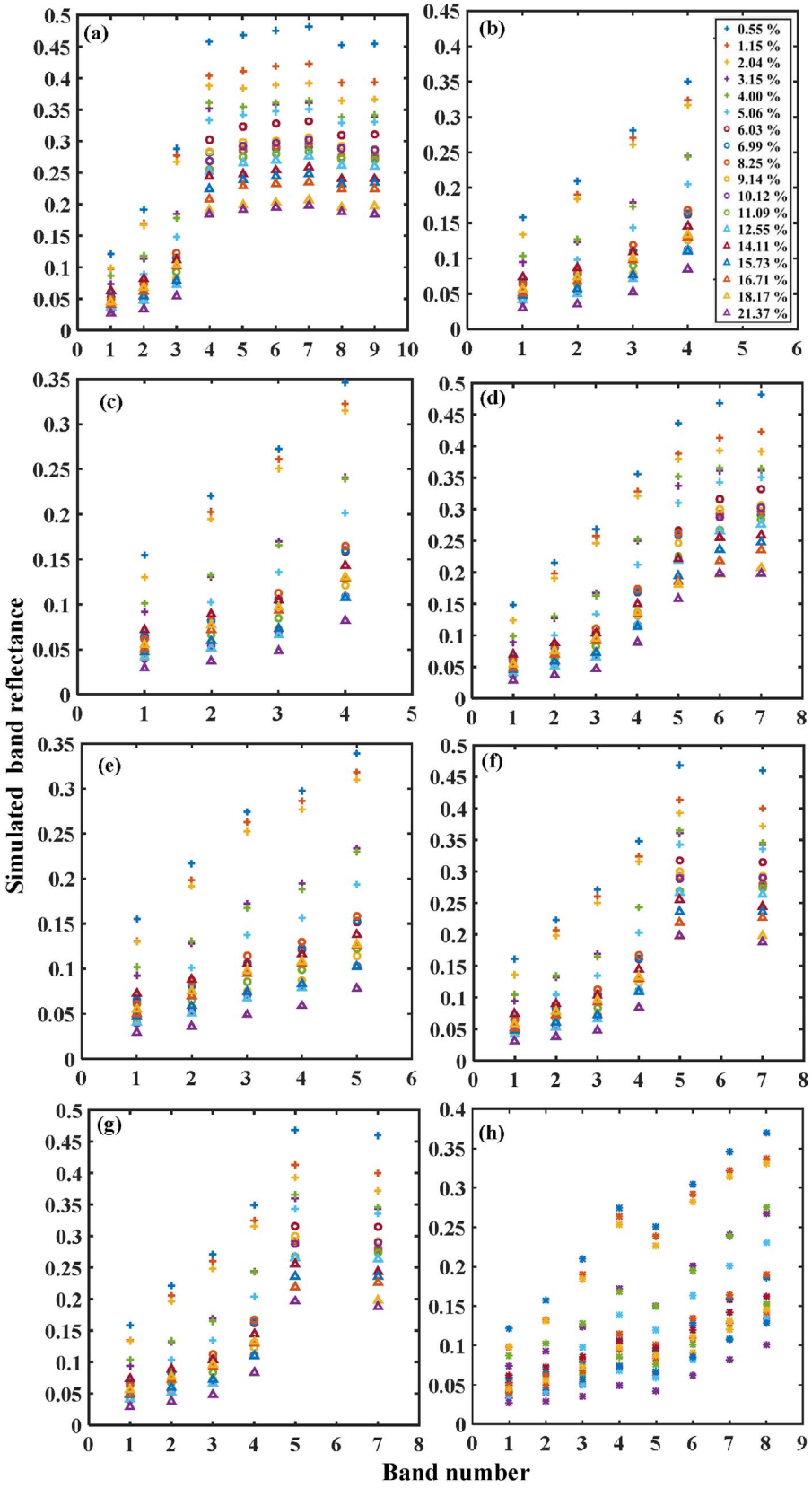

Fig. 2. Simulated band reflectance of various satellite sensors under different soil organic matter contents in the Sanjiang Plain: (a) ASTER; (b) GeoEye-1; (c) HJ-1A; (d) MODIS; (e) RapidEye; (f) Landsat TM5; (g) Landsat TM7; and (h) WorldView-2.

(ORI) and SOM differed for different simulated satellite data. Bands 3 and 4 had the highest correlation with SOM as follows: bands 3 and 4 for ASTER, GeoEye-1, and HJ-1A data; bands 3 and 5 for RapidEye, Landsat TM5, and Landsat TM7 data; bands 3 and 6 for MODIS data; and bands 4 and 8 for WorldView-2 data (Fig. 4, $R^2 > 0.20$). However, the spectral regions of bands from ASTER, MODIS, Landsat TM5, and Landsat TM7 and bands from GeoEye-1, HJ-1A, RapidEye, and WorldView-2 were very similar (Table S1). The best RI was observed for band 4 and band 8 in the simulated WorldView-2 data ($R^2 = 0.2965$ and RMSE = 2.739%, Table S2).

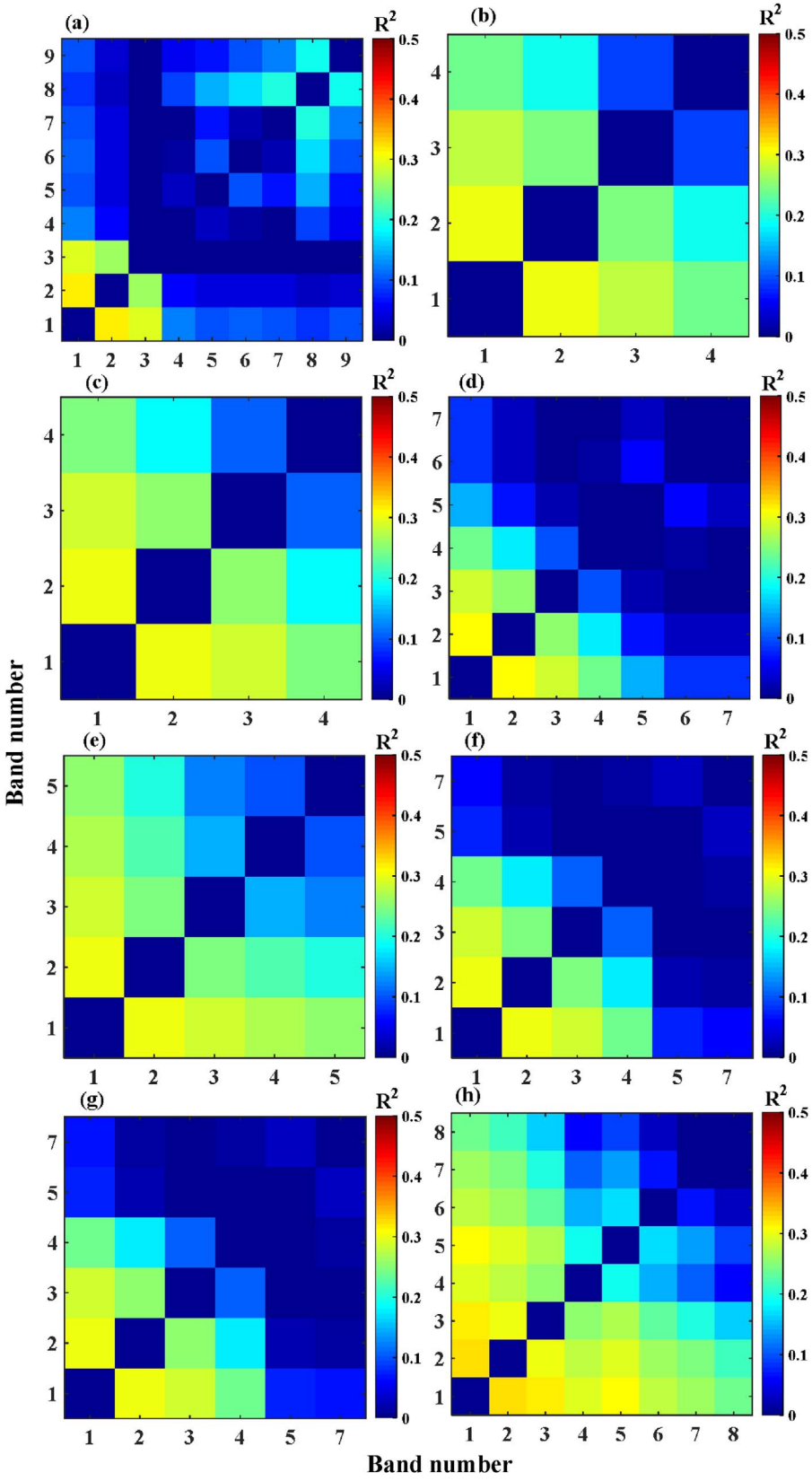

Fig. 3. Correlation between the optimal difference index (ODI) and soil organic matter content (SOM): (a) ASTER; (b) GeoEye-1; (c) HJ-1A; (d)MODIS; (e) RapidEye; (f)Landsat TM5; (g) Landsat TM7; and (h) WorldView-2.

The bands with the highest correlation between the optimal normalized difference vegetation index (ONDVI) and SOM also differed for different simulated satellite data. The most sensitive bands with the highest correlation with SOM were as follows: bands 3 and 4 for ASTER, GeoEye-1, and HJ-1A data; bands 3 and 5 for RapidEye data; bands 3 and 6 for MODIS, Landsat TM5, and Landsat TM7 data; and bands 1 and 2 for WorldView-2 data (Fig. 5, Table S2). The spectral regions of bands from GeoEye-1, HJ-1A, MODIS, RapidEye, Landsat TM5, and Landsat TM7 were very consistent, but those from ASTER and WorldView-2 differed (Table S1). The highest correlation between NDVI and SOM

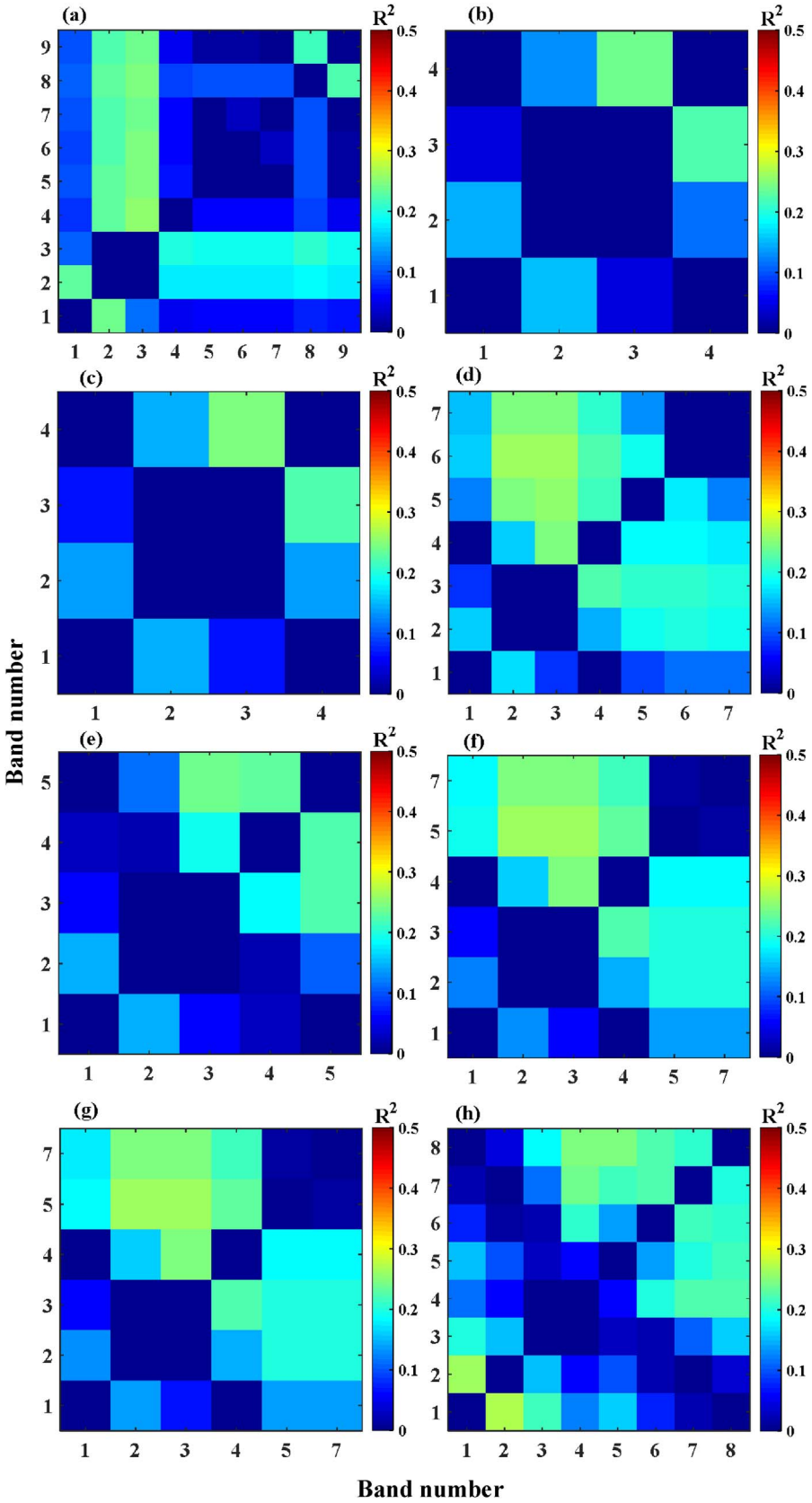

Fig. 4. Correlation between the optimal ratio index (ORI) and soil organic matter content (SOM): (a) ASTER; (b) GeoEye-1; (c) HJ-1A; (d) MODIS; (e) RapidEye; (f) Landsat TM5; (g) Landsat TM7; and (h) WorldView-2.

was obtained from the relation (band 1 − band 2)/(band 1 + band 2) for the simulated WorldView-2 data (R^2 = 0.2966 and RMSE = 2.737%, Table S2).

The optimal enhanced vegetation index (OEVI) was obtained by combing the three most highly correlated bands from each satellite with the optimal bands algorithm. The most highly correlated bands were bands 1 and 2 of all simulated satellite data. However, the spectral regions of different simulated satellite data had some differences (Table

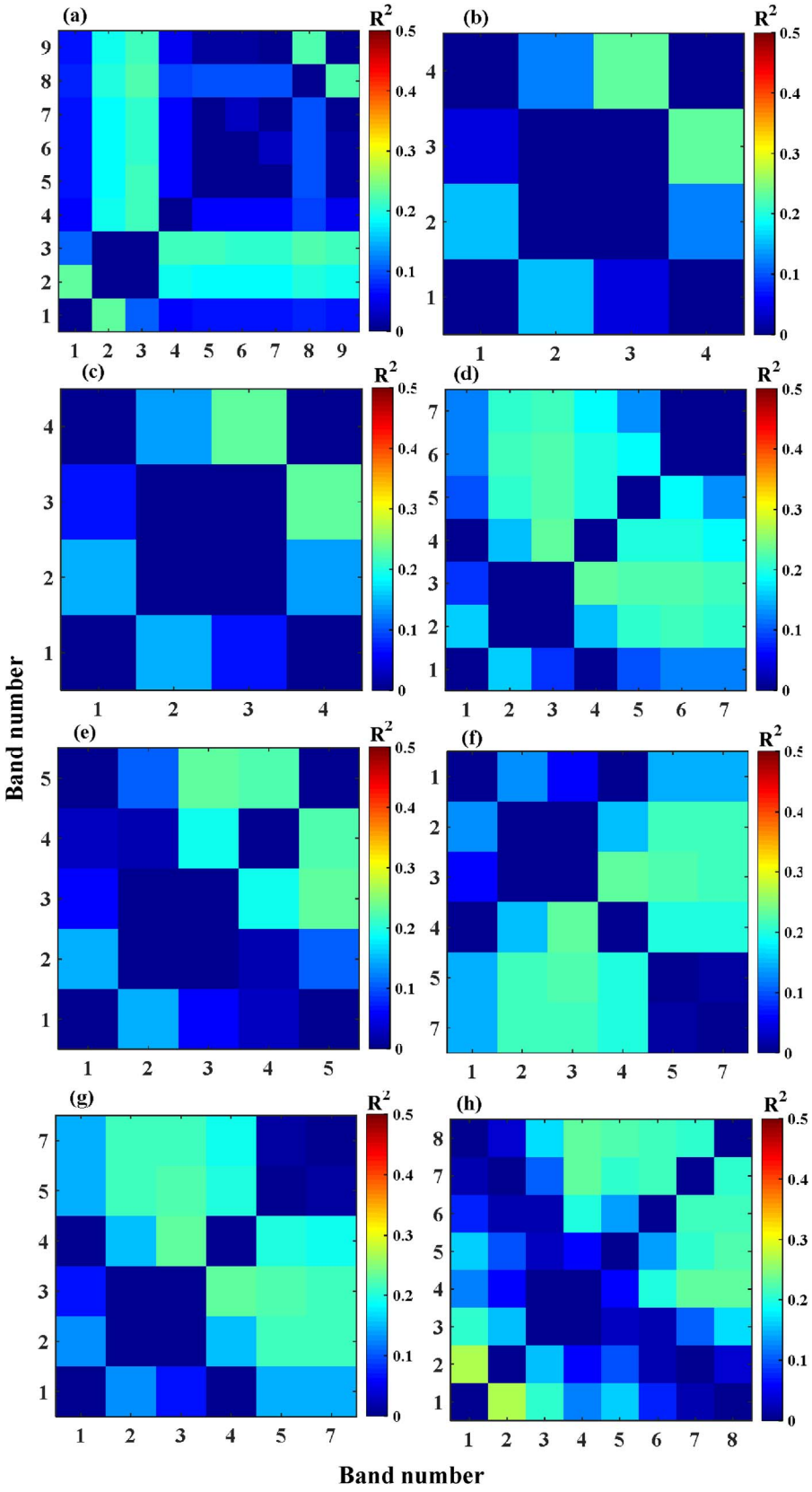

Fig. 5. Correlation between the optimal normalized difference vegetation index (ONDVI) and soil organic matter content (SOM): (a) ASTER; (b) GeoEye-1; (c) HJ-1A; (d) MODIS; (e) RapidEye; (f) Landsat TM5; (g) Landsat TM7; and (h) WorldView-2.

S1). The spectral regions of the GeoEye-1, HJ-1A, MODIS, RapidEye, Landsat TM5, and Landsat TM7 data were very consistent, but those of the ASTER and WorldView-2 data differed. The best OEVI was given by the expression (band 2 − band 1)/{[band 2 − (6 × band 1)] − (7.5 × band 1) + 1} × 2.5 in the simulated WorldView-2 data (R^2 = 0.43 and RMSE = 2.62%). The results showed that the SOM estimation accuracy was better using OEVI and ODI than using ORI and ONDVI for all satellite data (Table S2). Using ODI gave slightly lower SOM estimation accuracy than using OEVI, and using ONDVI gave slightly better SOM estimation accuracy than using ORI. The scatter

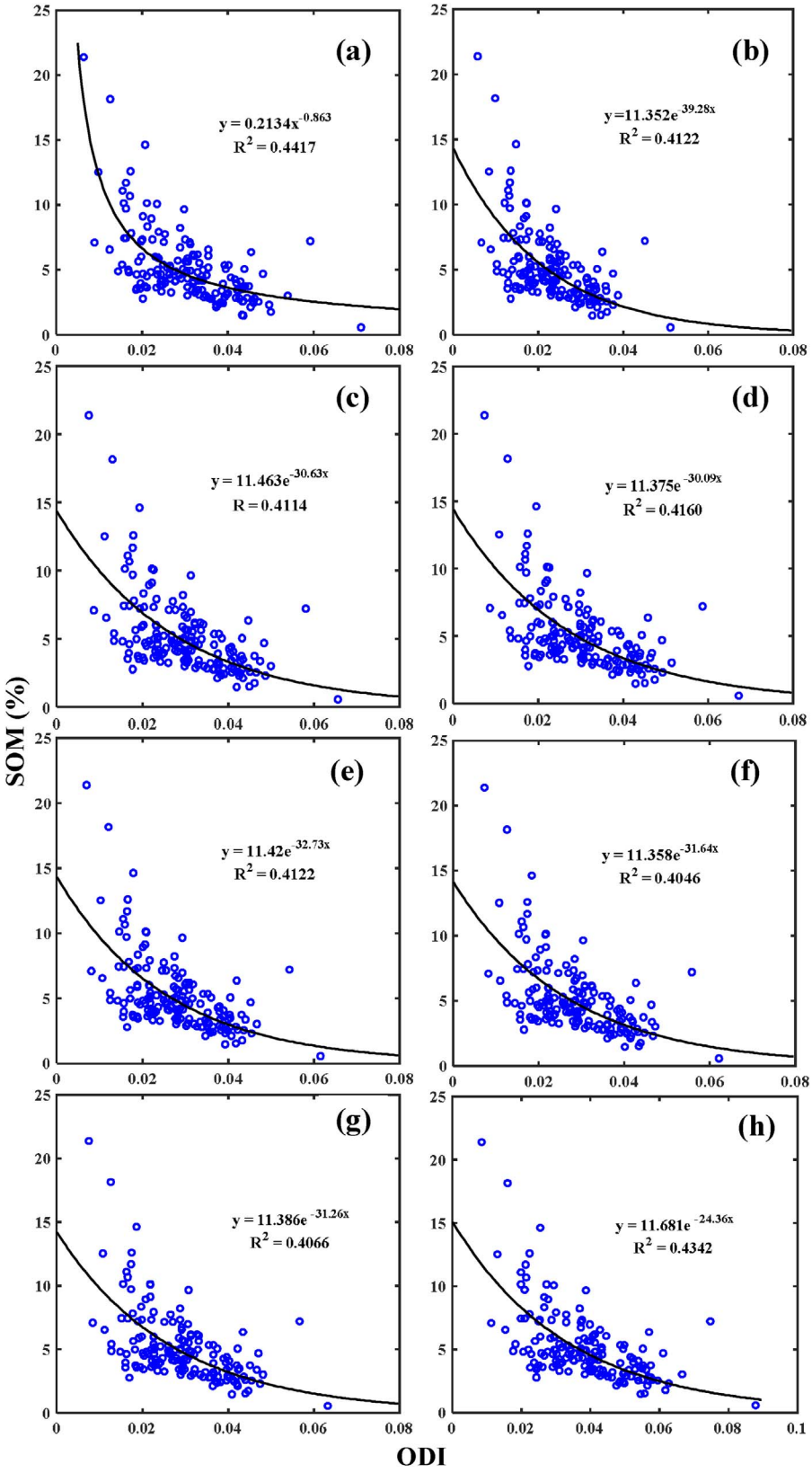

Fig. 6. Regression relationships between soil organic matter content (SOM) and the optimal difference index (ODI) for the following satellite data: (a) ASTER; (b) GeoEye-1; (c) HJ-1A; (d) MODIS; (e) RapidEye; (f) Landsat TM5; (g) Landsat TM7; and (h) WorldView-2.

plots of regression equations based on ODI, OEVI, and SOM for all simulated satellite data are presented in Figs. 6 and 7. The results indicate that the WorldView-2 data provided greater SOM estimation accuracy than data from other satellites (Figs. 3–5, Table S2).

3.3. Soil organic matter content estimation based on the combination of different simulated satellite data

We evaluated the feasibility and accuracy of SOM estimation using different simulated satellite data. All bands, ODI, ORI, ONDVI, and OEVI of each simulated satellite data were subjected to the particle

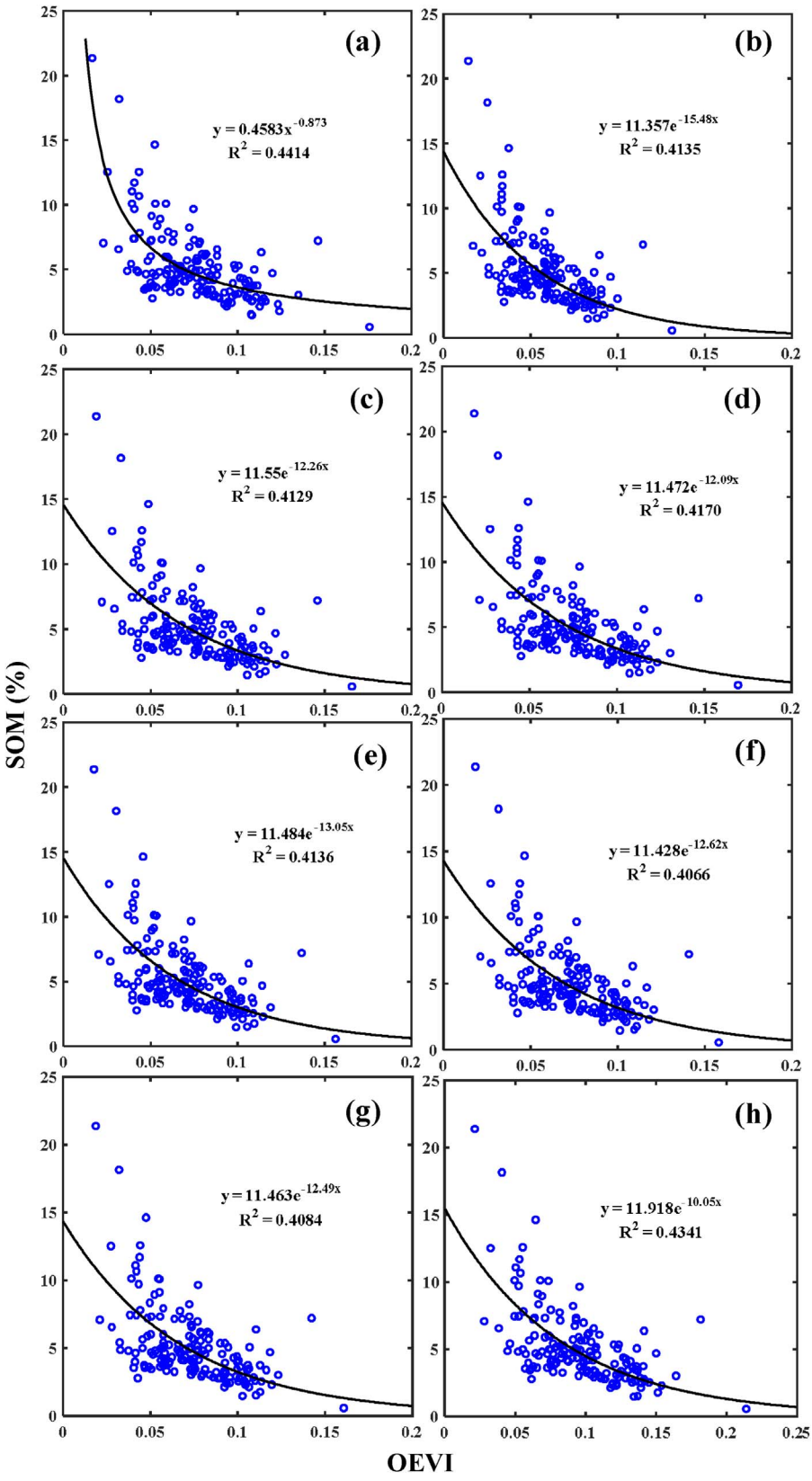

Fig. 7. Regression relationships between soil organic matter content (SOM) and the optimal enhanced vegetation index (OEVI) for the following satellite data: (a) ASTER; (b) GeoEye-1; (c) HJ-1A; (d) MODIS; (e) RapidEye; (f) Landsat TM5; (g) Landsat TM7; and (h) WorldView-2.

swarm optimization (PSO)-support vector machine (SVM) algorithm. The best SOM estimation accuracy was achieved using the simulated WorldView-2 data (R^2 = 0.77, RMSE = 1.66%, and AIC = 99.62, Table 1). The worst SOM estimation accuracy was obtained using the simulated HJ-1A data (R^2 = 0.67, RMSE = 1.87%, and AIC = 124.20 Table 1). In general, the order of SOM estimation accuracy (high to low) was achieved using WorldView-2, Landsat TM7, Landsat TM5, ASTER, MODIS, RapidEye, GeoEye-1, and HJ-1A data. The results indicated that there was a good relationship between the estimated SOM and the measured SOM (Fig. 8 and Table 1). The SOM estimation was

Table 1
Precision analyses for estimation models of soil organic matter content based on the PSO-SVM algorithm.

Satellite sensor	Dataset	Factor	R^2	RMSE (%)	AIC
ASTER	Calibration	13	0.74	1.52	161.87
	Validation	13	0.72	1.75	113.86
GeoEye-1	Calibration	8	0.68	1.64	175.33
	Validation	8	0.62	1.86	121.48
HJ-1A	Calibration	8	0.67	1.70	218.01
	Validation	8	0.61	1.87	124.20
MODIS	Calibration	11	0.72	1.60	174.81
	Validation	11	0.70	1.72	115.72
RapidEye	Calibration	9	0.70	1.62	170.02
	Validation	9	0.70	1.79	119.43
Landsat TM5	Calibration	10	0.73	1.56	147.24
	Validation	10	0.72	1.84	111.44
Landsat TM7	Calibration	10	0.73	1.53	137.57
	Validation	10	0.72	1.77	109.86
WorldView-2	Calibration	12	0.77	1.38	114.37
	Validation	12	0.76	1.66	99.62

sufficiently accurate when using the combination of all bands, ODI, ORI, ONDVI, and OEVI analyses of the satellite data subjected to the PSO-SVM algorithm.

The different simulated satellite data that had been comprehensively analyzed for satellite spectral region, spatial resolution, and revisit period was combined to further improve the SOM estimation accuracy and to enhance the applicability of different satellite data using the PSO-SVM algorithm. The ASTER data had a wider spectral region than that of other satellites, and ASTER bands 4–9 were sensitive to changes in SOM (Table S1; Dalal and Henry, 1986; Sudduth and Hummel, 1991; Palacio-Orueta and Ustin, 1998; Shepherd and Walsh, 2002; Daniel et al., 2004). Therefore, ASTER bands 4–9 were selected to provide alternative data for important missing bands of other satellites. Although the Geoeye 1, RapidEye, and WorldView-2 data had few bands, they had advantages of simultaneous spatial resolution and short revisit period. Therefore, data from Geoeye 1, RapidEye, and WorldView-2 were selected to combine with ASTER bands 4–9. HJ-A data also was selected to combine with ASTER bands 4–9 because of it had the advantage of relatively short revisit period. MODIS data had disadvantages in the spectral region and spatial resolution. Landsat TM5 and Landsat TM7 had disadvantages in the spectral region, spatial resolution, and revisit period. Therefore, the data from MODIS, Landsat TM5, and Landsat TM7 had less value for field-scale analyses, and were not combined with ASTER bands 4–9 for the PSO-SVM analysis.

The specific estimation accuracy of the combined result is presented in Table 2. The best relationship between the estimated SOM and the measured SOM was obtained from the combination of ASTER bands 4–9 and all bands, ODI, ORI, ONDVI, and OEVI of WorldView-2 (R^2 = 0.82, RMSE = 1.41%, and AIC = 82.86). The worst relationship between the estimated SOM and the measured SOM was obtained from the combination of ASTER bands 4–9 and all bands, ODI, ORI, ONDVI, and OEVI of HJ-1A (R^2 = 0.75, RMSE = 1.66%, and AIC = 105.60). The results indicated that the best estimates of SOM were very consistent with the measured SOM values (Fig. 9 and Table 2). The results suggested that the combination of ASTER bands 4–9 and all bands, ODI, ORI, ONDVI, and OEVI of GeoEye-1, HJ-1, RapidEye, and WorldView-2 could be used to further improve the SOM estimation accuracy.

4. Discussion

The results of this study showed that the simulated bands reflectance at the visible, near-infrared, and shortwave infrared regions were influenced by different SOM conditions in different satellite sensor data (Fig. 2). One of the main reasons for this is because the important simulated bands were in the same spectral regions as the main chemical groups and water absorption features of SOM, including C—H, S—H, N—H, O—H, C—N, and C—O (Gaffey et al., 1993). These spectral regions were located in the NIR and SWIR regions. In addition, the chromophorous groups were strongly related with SOM in the VIS region (Vasques et al., 2010). Our results were consistent with those of previous studies (Krishnan et al., 1980; Dalal and Henry, 1986; Palacio-Orueta and Ustin, 1998; Shepherd and Walsh, 2002; Daniel et al., 2004; McCarty and Reeves, 2006; Liu et al., 2009; Kweon and Maxton, 2013; Jin et al., 2016). The results suggested that the reflectance changes of the simulated bands in the VIS, NIR, and SWIR regions could be used to estimate SOM.

The results showed that the indexes from the different simulated satellite data were highly correlated with SOM (Figs. 3–5 and Table S2); ORI and ONDVI were positively correlated while ODI and OEVI were negatively correlated (Figs. 6 and 7). The highest spectral reflectance values were observed at 0.55% SOM (Fig. 2). Previous results have indicated that spectral characteristics can be used to accurately estimate low SOM values in areas undergoing desertification (R^2 = 0.88 and RMSE = 0.48%, Gao et al., 2011). In addition, remote sensing data can be used to analyze the relationship between low SOM and low vegetation on various spatial scales. The selected ODI bands were bands 1 and 2 (Fig. 3). However, the important ODI spectral regions were 0.430-0.520 μm and 0.510 − 0.600 μm, except for those of ASTER (band 1, 0.520-0.600 μm and band 2, 0.630-0.690 μm), MODIS (band 1, 0.459-0.0.479 μm and band 2, 0.545-0.565 μm), and WorldView-2 (band 1, 0.400-0.450 μm and band 2, 0.45-0.510 μm) (Table S1). The selected most sensitive bands of ORI had some differences (Fig. 4 and Table S2), but the selected spectral regions of ASTER, MODIS, Landsat TM5, and Landsat TM7 data and the spectral regions of GeoEye-1, HJ-1A, RapidEye, and WorldView-2 data were very similar (Table S1). The selected most sensitive bands for ONDVI were bands 3 and 4, and the selected spectral regions were very consistent, except for the selected bands and spectral regions of RapidEye and WorldView-2 (Fig. 5 and Table S2). The selected bands of OEVI were the same (bands 1 and 2), but their spectral regions differed in different satellite data (Tables S1 and S2). These combined results showed that the ODI and OEVI spectral regions were located in the VIS and NIR regions (these bands were very sensitive to SOM) in the different simulated satellite data. The spectral regions of ORI and ONDVI were partly located in the SWIR region (primarily the water absorption band; , Tables S1 and S2).

In this study, the spectral regions that were sensitive to changes in SOM were located in the VIS and NIR regions, which is consistent with previous reports (Bowers and Hanks, 1965; Krishnan et al., 1980; Dalal and Henry, 1986; Palacio-Orueta and Ustin, 1998; Hummel et al., 2001; Daniel et al., 2004; McCarty and Reeves, 2006; Liu et al., 2009; Qi et al., 2014; Jin et al., 2016). The results showed that the SOM estimation accuracy was better using the ODI and OEVI model than using the ORI and ONDVI model (Table S2). The main reason for this was because the spectral regions of ODI and OEVI were more sensitive to changes in SOM than the spectral regions of ORI and ONDVI, which was determined by the indirect correlation between SOM and soil water content. The results also indicated that the ODI, ORI, ONDVI, and OEVI analyses of WorldView-2 data had the highest correlation with measured SOM values (Table S2), possibly because all WorldView-2 bands were located in the VIS and NIR regions, and were not significantly affected by atmospheric water absorption. The results suggested that the WorldView-2 data were superior for SOM estimation compared to data from other satellites.

The sensitivity of the spectral regions to SOM varied with different soil types (Jin et al., 2016). These results showed that the soil spectral reflectance was highly correlated with SOM in the study region of Northeast China. The spatial changes of soil properties and soil genesis may result in the uncertainty of SOM estimation results. In the current study, the spatial changes of soil properties and soil genesis were not considered, which may reduce the SOM estimation accuracy. Therefore, the stability of the SOM estimation model may be further improved in future studies by analyzing the relationships between SOM and spatial

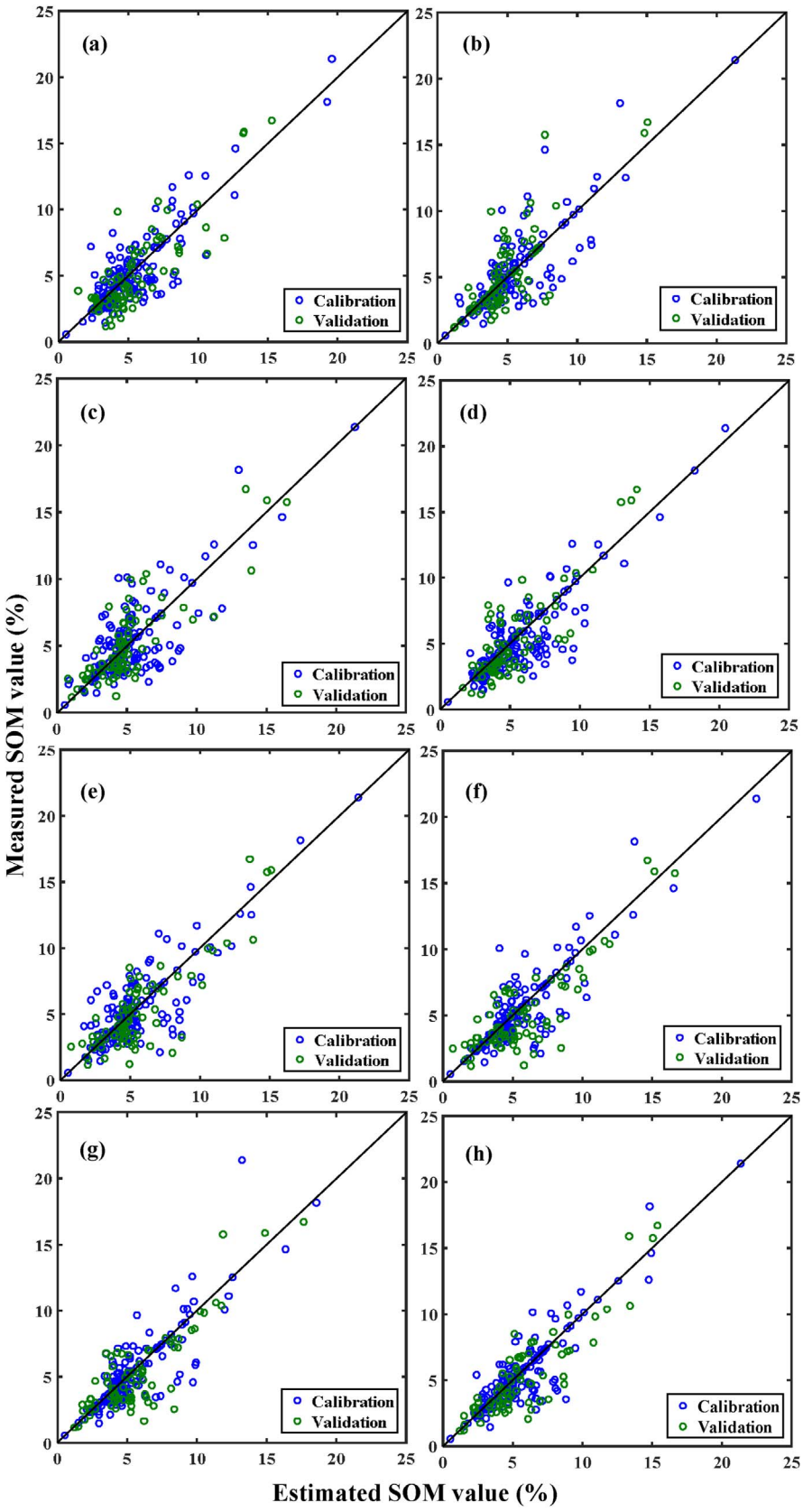

Fig. 8. Relationships between measured and estimated soil organic matter content (SOM) values using the following satellite data: (a) ASTER; (b) GeoEye-1; (c) HJ-1A; (d) MODIS; (e) RapidEye; (f) Landsat TM5; (g) Landsat TM7; and (h) WorldView-2.

changes of soil properties and soil genesis. In this study, the different simulated satellite data were used to estimate SOM. The developed methodology will provide a useful guideline for estimating SOM using suitable satellite data in black-soil regions.

All spectral bands, ODI, ORI, ONDVI, and OEVI of the each simulated satellite data were subjected to the PSO-SVM algorithm to estimate SOM. Although the selected factors differed in the different simulated satellite data, the results identified good relationships between

Table 2
Combination of different satellite sensor data for estimation models of soil organic matter content based on PSO-SVM algorithms.

Satellite sensor	Dataset	Factor	R^2	RMSE (%)	AIC
ASTER(B4-B9) + GeoEye-1	Calibration	14	0.75	1.40	132.76
	Validation	14	0.73	1.65	107.62
ASTER(B4-B9) + HJ-1	Calibration	14	0.75	1.41	138.95
	Validation	14	0.74	1.66	105.60
ASTER(B4-B9) + RapidEye	Calibration	15	0.79	1.33	127.54
	Validation	15	0.75	1.58	100.51
ASTER(B4-B9) + WorldView-2	Calibration	18	0.82	1.21	90.82
	Validation	18	0.80	1.41	82.86

the estimated and measured SOM in the Sanjiang Plain (R^2 = 0.61-0.77, RMSE = 1.38-1.87%, AIC = 99.62–218.01; Fig. 8 and Table 1). The results indicated that data from the eight satellite sensors (ASTER, Geoeye 1, HJ-1A, MODIS, RapidEye, Landsat TM5, Landsat TM7, and WorldView-2) could be analyzed by the PSO-SVM algorithm to estimate SOM. Our comprehensive consideration of different satellite data, spectral regions, spatial resolution, and revisit period indicated that ASTER bands 4–9, and all bands, ODI, ORI, ONDVI, and OEVI of GeoEye-1, HJ-1, RapidEye, and WorldView-2 could be combined to improve the SOM estimation accuracy obtained with the PSO-SVM algorithm. The SOM estimation accuracy was improved by combining data from different satellites rather than using data from a single satellite (R^2 = 0.73-0.82, RMSE = 1.21-1.65%, and AIC = 82.86-138.95; Fig. 9 and Table 2). Our results were consistent with those of previous studies (Abdikan et al., 2014; Xu et al., 2015; Jin et al., 2015). Compared with RMSE and R^2, AIC is a better parameter for measuring the goodness of fit of a multiple parameter statistical model. This is because AIC accounts for the trade-off between bias and variance in model construction (Arnold, 2010). Thus, AIC should be employed to evaluate estimation accuracy when a multiple parameter statistical model is used to estimate SOM.

The results showed that the combination of ASTER and WorldView-2 data provided the greatest SOM estimation accuracy because the spectral region, spatial resolution, and revisit period were very sensitive to SOM (R^2 = 0.82, RMSE = 1.41%, and AIC = 82.86; Fig. 9 and Table 2). These results indicated that the PSO-SVM algorithm was a useful tool for estimating SOM. The PSO algorithm was used to find the optimal values for the two parameters (C and γ) of SVM, which improved the estimation accuracy of the SVM model. The use of the kernel function and the SVM model also helped to simplify the complex calculations (Vapnik, 2013). Therefore, POS and SVM were combined to estimate SOM. The results showed that the SOM estimation results of the PSO-SVM algorithm were more accurate than those obtained from

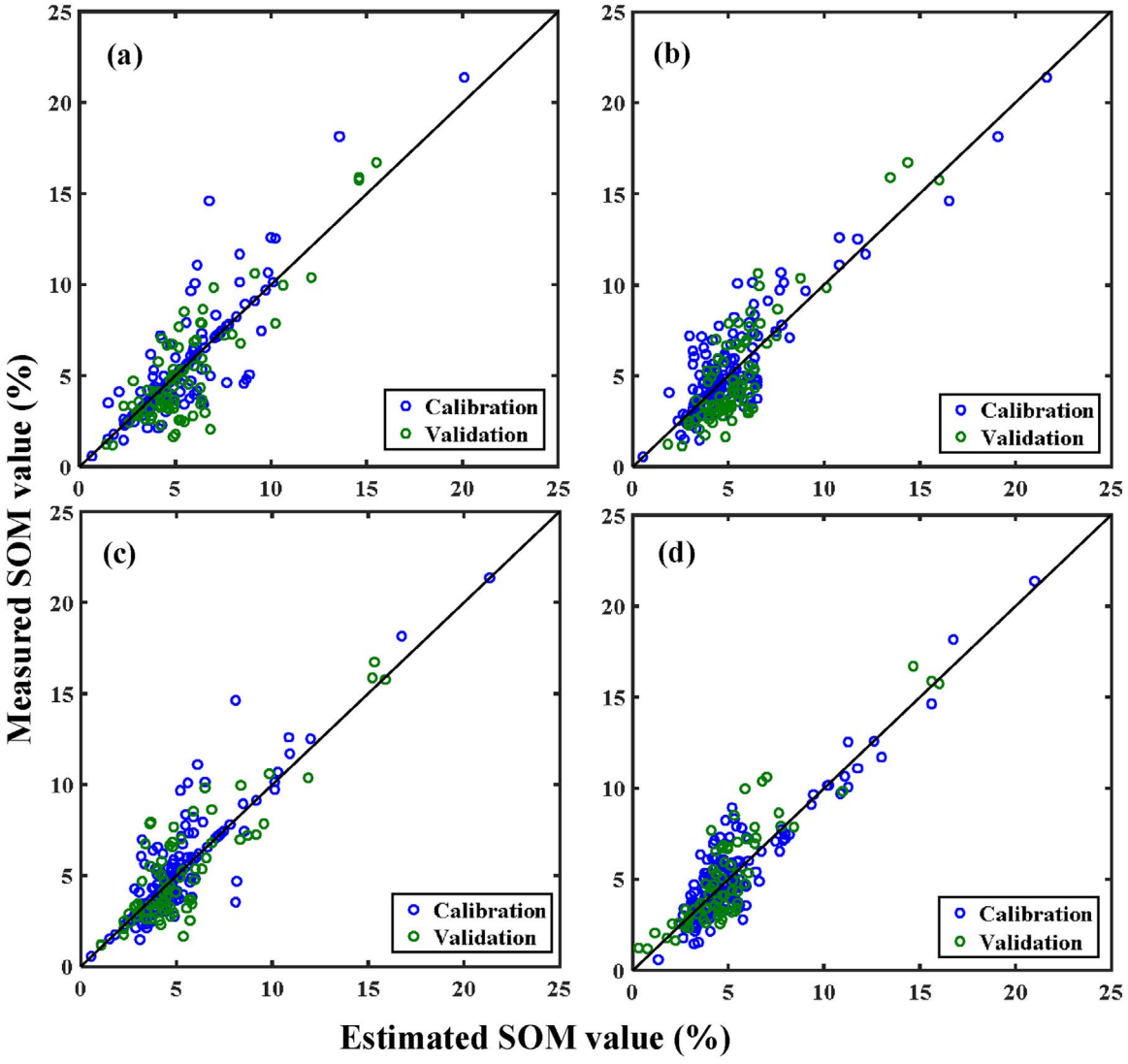

Fig. 9. Relationships between measured and estimated soil organic matter content (SOM) values: (a) ASTER (B4 − B9) + GeoEye-1; (b) ASTER (B4 − B9) + HJ-1; (c) ASTER (B4 − B9) + RapidEye; and (d) ASTER (B4 − B9) + WorldView-2.

the optimal band algorithm (Tables 1, 2, and S2). The PSO-SVM algorithm increased the sensitivity of spectral bands to SOM changes because it considered many SOM-related spectral bands. Each SOM-related spectral band had a complementary band (Jin et al., 2016), such as soil water content, which further improved the SOM estimation accuracy by taking into account the effect of soil water content on reducing reflectance.

This study showed that a combination of different algorithms can increase the estimation accuracy of soil parameters. The PSO-SWM algorithm required the effect of soil water content on satellite reflectance to be taken into account resulting in superior estimates of SOM at field scale. We used different simulated satellite data to estimate SOM and obtained good accuracy. This study was focused on the comparison of different satellite bands and vegetation indices for estimating soil organic matter based on simulated spectral configuration. We did not consider the effect of the different spatial resolution of remote sensing imagery on the estimation accuracy of SOM and future studies should investigate this topic. The actual satellite data and the simulated satellite data differ because the actual satellite data is influenced by the atmospheric environment. Therefore, actual satellite data should be used in future studies to evaluate the SOM estimation model.

5. Conclusion

In this study, the optimal bands algorithm and the PSO-SVM algorithm were used to select the best regression model for estimating SOM with different simulated satellite data. The results showed that the band reflectance of different simulated satellite data had similar spectral shapes under different SOM, but were influenced by differences in SOM. The band reflectance gradually decreased with increasing SOM in all bands of the different simulated satellite data. The results showed that 0.55% and 21.37% SOM had the highest and lowest values of spectral reflectance, respectively. The best SOM estimation accuracy was achieved by OEVI in the simulated WorldView-2 data (R^2 = 0.4341 and RMSE = 2.623%) using the optimal bands algorithm. The SOM estimation accuracy was better for ODI and OEVI than for ORI and ONDVI in the different simulated satellite data. SOM was estimated using all bands, ODI, ORI, ONDVI, and OEVI of each simulated satellite data. The best SOM estimation accuracy was obtained from the simulated WorldView-2 data (R^2 = 0.77, RMSE = 1.66%, and AIC = 99.62) using the PSO-SVM algorithm. The strongest correlation between the estimated SOM and the measured SOM was obtained from the combination of ASTER bands 4–9 and all bands, ODI, ORI, ONDVI, and OEVI of WorldView-2 (R^2 = 0.82, RMSE = 1.41% and AIC = 82.86) using the PSO-SVM algorithm. The results showed that the SOM estimation accuracy was highest using all bands, ODI, ORI, ONDVI, and OEVI of the WorldView-2 data and the combination of ASTER bands 4 − 9 and all bands, ODI, ORI, ONDVI, and OEVI of HJ-1A and GeoEye-1.

Acknowledgements

This study was jointly supported by the National Basic Research Program of China (No. < GN1 > 2013CB430401 < GN1 >), < GS2 > the National Natural Science Foundation of China < GS2 > (No. < GN2 > 41601369 < GN2 >) and the “One Hundred Talents” program from Chinese Academy of Sciences granted to Dr. Kaishan Song. The authors thank the anonymous reviewers and the editor in charge for their efforts, which have strengthened this manuscript.

Appendix A. Supplementary data

Supplementary data associated with this article can be found, in the online version, at http://dx.doi.org/10.1016/j.agrformet.2017.05.018.

References

Abdikan, S., Sanlia, F.B., Sunar, F., Ehlers, M., 2014. A comparative data-fusion analysis of multi-sensor satellite images. Int. J. Digit. Earth 7, 671–687.
Arnold, T.W., 2010. Uninformative parameters and model selection using Akaike's Information Criterion. J. Wildl. Manage. 74, 1175–1178.
Baumgardner, M.F., Silva, L.F., Biehl, L.L., Stoner, E.R., 1985. Reflectance properties of soils. Adv. Agron. 38, 1–44.
Bowers, S.A., Hanks, R.J., 1965. Reflectance of radiant energy from soils. Soil Sci. 100, 130–138.
Brown, D.J., Shepherd, K.D., Walsh, M.G., Dewayne Mays, M., Reinsch, T.G., 2006. Global soil characterization with VNIR diffuse reflectance spectroscopy. Geoderma 132, 273–290.
Dalal, R.C., Henry, R.J., 1986. Simultaneous determination of moisture, organic carbon and total nitrogen by near infrared reflectance spectrophotometry. Soil Sci. Soc. Am. J. 50, 120–123.
Daniel, K.W., Tripathi, N.K., Honda, K., Apisit, E., 2004. Analysis of VNIR (400–1100 nm) spectral signatures for estimation of soil organic matter in tropical soils of Thailand. Int. J. Remote Sens. 25, 643–652.
Eberhart, R.C., Shi, Y., 2001. Particle swarm optimization: developments, applications and resources. Proceedings of the International Congress on Evolutionary Computation 81–86.
Fleming, K.L., Heermann, D.F., Westfall, D.G., 2004. Evaluating soil color with farmer input and apparent soil electrical conductivity for management zone delineation. Agron. J. 96, 1581–1587.
Gaffey, S.J., McFadden, L.A., Nash, D., Pieters, C.M., 1993. Ultraviolet, visible, and near-infrared reflectance spectroscopy: laboratory spectra of geologic materials. In: Pieters, C.M., Englert, P.E. (Eds.), Remote Geochemical Analysis: Elemental and Mineralogical Composition. Cambridge Univ. Press, Cambridge, UK, pp. 43–77.
Gao, Z.H., Bai, L.N., Wang, B.Y., Li, Z.Y., Li, X.S., Wang, Y.K., 2011. Estimation of soil organic matter content in desertified lands using measured soil spectral data. Sci. Silvae Sin. 47, 9–16 (in Chinese).
Guo, Y., Ji, W.J., Wu, H.H., Shi, Z., 2013. Estimation and mapping of soil organic matter based on Vis-NIR reflectance spectroscopy. Spectrosc. Spect. Anal. 33, 1135–1140 (in Chinese).
Hummel, J.W., Sudduth, K.A., Hollinger, S.E., 2001. Soil moisture and organic matter prediction of B-horizon soils using an NIR soil sensors. Comput. Electron. Agr. 32, 149–165.
Irons, J.R., Weismiller, R.A., Petersen, G.W., 1989. Soil reflectance. In: Asrar, G. (Ed.), Theory and Applications of Optical Remote Sensing. John Wiley and Sons, NewYork, USA, pp. 66–106.
Jin, X.L., Xu, X.G., Song, X.Y., Li, Z.H., Wang, J.H., Guo, W.S., 2013. Estimation of leaf water content in winter wheat using grey relational analysis (GRA)-partial least squares (PLS) modeling with hyperspectral data. Agron. J. 105, 1385–1392.
Jin, X.L., Yang, G.J., Xu, X.G., Yang, H., Feng, H.K., Li, Z.H., Shen, J.X., Zhao, C.J., Lan, Y.B., 2015. Combined multi-temporal optical and radar parameters for estimating LAI and biomass in winter wheat using H J and Radarsat-2 data. Remote Sens. 7, 13251–13272.
Jin, X.L., Du, J., Liu, H.J., Wang, Z.M., Song, K.S., 2016. Remote estimation of soil organic matter content in the Sanjiang Plain: northest China: the optimal band algorithm versus the GRA-ANN model. Agric. For. Meteorol. 218–219, 250–260.
Kennedy, J., Eberhart, R.C., 1995. Particle swam optimization. Proceedings of IEEE International Conference on Neural Networks 1942–1948.
Krishnan, P., Alexander, J.D., Butler, B., Hummel, J.W., 1980. Reflectance technique for predicting soil organic matter. Soil Sci. Soc. Am. J. 44, 1282–1285.
Kweon, G., Maxton, C., 2013. Soil organic matter sensing with an on-the-go optical sensor. Biosyst. Eng. 115, 66–81.
Liu, H., Zhang, Y., Zhang, B., 2009. Novel hyperspectral reflectance models for estimating black-soil organic matter in northeast china. Environ. Monit. Assess. 154, 147–154.
Liu, S.L., An, N.N., Yang, J.J., Dong, S.K., Wang, C., Yin, Y.J., 2015. Prediction of soil organic matter variability associated with different land use types in mountainous landscape in southwestern Yunnan province, China. Catena 133, 137–144.
McCarty, G.W., Reeves, J.B., 2006. Comparisons of near infrared and mid infrared diffuse reflectance spectroscopy for field-scale measurement of soil fertility parameters. Soil Sci. 171, 94–102.
O'Kelly, B.C., 2004. Accurate determination of moisture content of organic soils using the oven drying method. Dry. Technol. 22, 1767–1776.
Palacio-Orueta, A., Ustin, S.L., 1998. Remote sensing of soil properties in the Santa Monica mountains I Spectral analysis. Remote Sens. Environ. 65, 170–183.
Prescott, C.E., Maynard, D.G., Laiho, R., 2000. Humus in northern forests: friend or foe? For. Ecol. Manag. 133, 23–36.
Qi, Y.Q., Lv, X., Shao, Y.L., Feng, B., Chen, J., Li, X.W., Zhang, Z., 2014. Study on soil organic matter content estimated model by hyperspectral remote sensing data. Xinjiang Agric. Sci. 51, 1300–1305 (in Chinese).
Rinnan, Å., van den Berg, F., Engelsen, S.B., 2009. Review of the most common pre-processing techniques for near-infrared spectra. TrAC Trend Anal. Chem. 28, 1201–1222.
Rossel, R.A.V., Walvoort, D.J.J., McBratney, A.B., Janik, L.J., Skjemsta, J.O., 2006. Visible, near infrared, mid infrared or combined diffuse reflectance spectroscopy for simultaneous assessment of various soil properties. Geoderma 131, 59–75.
Seely, B., Welham, C., Blanco, J.A., 2010. Towards the application of soil organic matter as an indicator of forest ecosystem productivity:deriving thresholds, developing monitoring systems, and evaluating practices. Ecol. Indic. 5, 999–1008.
Shepherd, K.D., Walsh, M.G., 2002. Development of reflectance spectral libraries for characterization of soil properties. Soil Sci. Soc. Am. J. 66, 988–998.

Six, J., Paustian, K., 2014. Aggregate-associated soil organic matter as an ecosystem property and a measurement tool. Soil Biol. Biochem. 68, A4–A9.
Stamatiadis, S., Christofides, C., Tsadilas, C., Samaras, V., Schepers, J.S., Francis, D., 2005. Groundsensor soil reflectance as related to soil properties and crop response in a cotton field. Precis. Agric. 6, 399–411.
Sudduth, K.A., Hummel, J.W., 1991. Evaluation of reflectance methods for soil and soil organic matter sensing. Trans. ASAE 34, 1900–1909.
Vapnik, V.N., Vapnik, V., 1998. Statistical Learning Theory. John Wiley and Sons, New York, USA.
Vapnik, V., 2013. The Nature of Statistical Learning Theory. Springer Science & Business Media.
Vasques, G.M., Grunwald, S., Harris, W.G., 2010. Spectroscopic models of soil organic carbon in Florida, USA. J. Environ. Qual. 39, 923–934.
Xie, B.C., Xue, X.Z., Liu, W.D., Wang, J.H., Wang, G.D., 2005. Hull-curve-method-based extraction and analysis of soil spectral characteristics. ActaPedol. Sin. 42, 171–175 (in Chinese).
Xu, B.B., Dai, C.D., 1980. The correlation between Nanjiang soil spectral reflectance property and organic matter. Chin. Sci. Bull. 6, 282–284 (in Chinese).
Xu, Y., Ma, P.F., Ng, E., Lin, H., 2015. Fusion of world view-2 stereo and multitemporal terra SAR-X images for building height extraction in urban areas. IEEE Geosci. Remote S. 12, 1795–1799.
Zhou, P., Wang, R.S., Yan, B.K., Yang, S.M., Wang, Q.H., 2008. Extraction of soil organic matter information by hyperspectral remote sensing. Prog. Geogr. 27, 27–34.